

Observation of Anomalous Spin Torque Generated by a Ferromagnet

Arnab Bose,^{1,*} D. D. Lam,^{2,†} S. Bhuktare,¹ S. Dutta,¹ H. Singh,¹ Y. Jibiki,² M. Goto,²
S. Miwa,² and A. A. Tulapurkar^{1,‡}

¹*Department of Electrical Engineering, Indian Institute of Technology Bombay,
Powai, Mumbai 400 076, India*

²*Graduate School of Engineering Science, Osaka University, Toyonaka, Osaka 560-8531, Japan*

 (Received 25 October 2017; revised manuscript received 12 March 2018; published 18 June 2018)

The spin-transfer-torque effect is predicted and subsequently demonstrated in a giant magnetoresistive (GMR) structure with current-perpendicular-to-plane geometry. In this work, we report that an unconventional out-of-plane magnetic field is created and exerts torque on a free magnet while in-plane current flows through the GMR sample. This strong effective magnetic field completely dominates the dampinglike torque which is expected to arise due to the anomalous Hall effect of a ferromagnet (analogous to the spin Hall effect in heavy metal). This anomalous magnetic field shows a very unusual angular dependence, which indicates broken-mirror symmetry in the lateral dimension. This anomalous torque may open an additional functionality for memory application.

DOI: [10.1103/PhysRevApplied.9.064026](https://doi.org/10.1103/PhysRevApplied.9.064026)

I. INTRODUCTION

Over the years, the central research of spintronics has been focused on generating spin current [1–5] and an effective field [6–9] to control the magnetization dynamics by spin torques [10–16]. Spin-orbit interaction-induced torques (SOTs) have drawn considerable interest in recent years [6–17]. In most cases, dampinglike torque is created when a ferromagnet absorbs spin current generated by the spin Hall effect (SHE), and fieldlike torque (FLT) is created by a Rashba-Dresselhaus interaction or an Oersted field. Up to now, the study of SOT is limited to systems consisting of nonmagnet (NM) and ferromagnet (FM) where the NM has a large spin-orbit coupling (such as Pt, W, etc.) [5–13,18–25]. In this work, we show that nonmagnets are not the only the source to produce SOTs, but a ferromagnet can also generate a significant amount of torque on another ferromagnet owing to its spin-orbit interaction.

The FM has its own spin-orbit coupling which is responsible for various effects such as anisotropic magnetoresistance (AMR), the anomalous Hall effect (AHE), and the planar Hall effect (PHE) [23]. The AHE in a FM is analogous to the SHE in a heavy metal (HM) [Fig. 1(a)]. Previous studies show that the spin Hall angle of a FM [26–28] is comparable to Pt. Hence, a FM can be

considered as a good source for SOTs. To study the spin-orbit torque generated by a FM, a FM(free)/Cu/FM(fixed) heterostructure is required, where the fixed layer will be a source of spin current or an effective field which will exert torque on a free FM which is separated by a Cu spacer from the fixed layer [inset in Fig. 1(b)]. Based on this fact, we carry out a spin-torque ferromagnetic resonance (STFMR) [13,18–24] measurement on a giant magnetoresistive (GMR) stack with current-in-plane (CIP) geometry [Fig. 1(c)]. We surprisingly observe a kind of torque which is completely different from conventional spin-orbit torque by a FM (owing to its AHE) which we expected earlier. This unconventional spin torque depends on the mutual orientation of the fixed-layer magnetization direction (\mathbf{M}) and the direction of in-plane current flow (\mathbf{J}) and manifests itself as an effective magnetic field perpendicular to both \mathbf{M} and \mathbf{J} . This is also markedly different from the spin torques observed in current-perpendicular-to-plane devices, where the spin torque depends only on the angle between the directions of free- and fixed-layer magnetizations [10]. This anomalous magnetic field may open up a possibility to switch high-density perpendicular magnetic bits for memory application [29–31].

II. SAMPLE PREPARATION

A GMR film is grown on a thermally oxidized SiO₂ wafer by sputtering in argon ambient with a base pressure better than 4×10^{-9} Torr with the following metals: Ta(5)/Ru(5)/InMn(7)/CoFe(2)/Cu(5)/CoFe(2)/Cu(5) (numbers in brackets are in nanometers). Magnetization of

*arnabbose@ee.iitb.ac.in

†Present address: Institute of Materials Science (IMS), VAST, Vietnam and Graduate University of Science and Technology (GUST), VAST, Vietnam.

‡ashwin@ee.iitb.ac.in

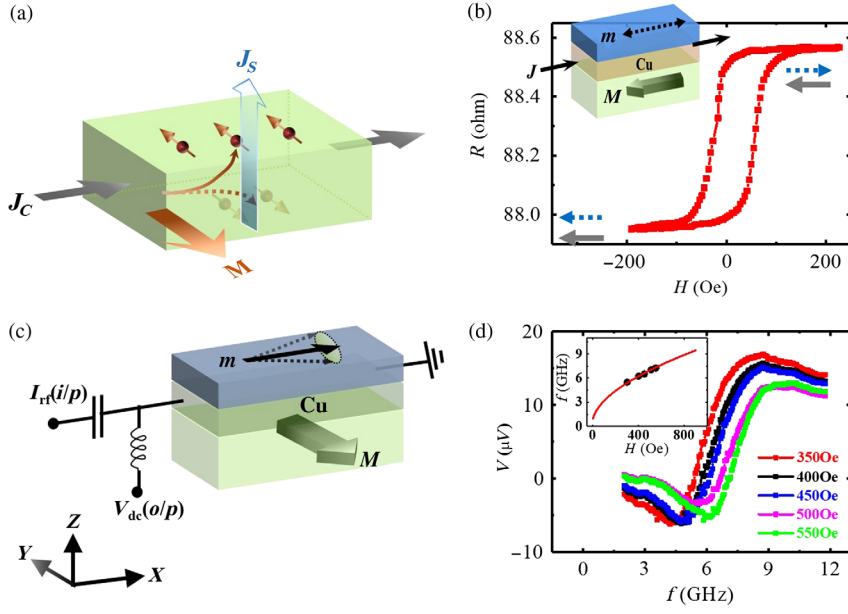


FIG. 1. (a) Generation of spin current (J_S) by the AHE. (b) Electrical characterization of a GMR stack. The inset in (b) shows the schematics of a GMR stack. (c) Schematic description of the STFMR experiment. (d) Experimental data of the STFMR experiment for different applied external magnetic fields applied along the X axis. The inset shows the resonance frequency as a function of the magnetic field.

the bottom ferromagnet $\text{Co}_{70}\text{Fe}_{30}$ is pinned by annealing the sample at 300°C for 2 h in an external in-plane magnetic field of 0.6 T. The top $\text{Co}_{70}\text{Fe}_{30}$ is a free layer which is protected by 5 nm of Cu cap. The stack is patterned to a rectangular shape ($375\ \mu\text{m} \times 25\ \mu\text{m}$) by optical lithography and argon ion milling.

III. CHARACTERIZATION TECHNIQUE

Figure 1(b) shows the dc-electrical characterization of a GMR stack with CIP geometry in which current is passed in the plane of the sample while the field is swept along the direction of the fixed layer [inset in Fig. 1(b)]. It clearly shows two distinct values of resistance, confirming the dominant in-plane GMR effect over other effects (such as AMR, PHE, etc.) [Fig. 1(b)]. The low- and high-resistance states correspond to the parallel and antiparallel alignments of the fixed- (M) and free-layer magnetization (m), respectively. The STFMR technique is used to measure spin torques in this device. In-plane radio frequency (rf) current is passed and voltage is measured as shown in Fig. 1(c), while the frequency is swept in the presence of a constant external magnetic field. For a FM-HM structure, generally the magnetic field is swept to measure STFMR [13,18–24], but a frequency sweep [32–35] is favorable in the case of a GMR and magnetic tunnel junctions structure, since the fixed layer can also move at a higher magnetic field, leading to an erroneous result. On the application of a rf current, the free-layer magnetization undergoes precession due to the Oersted magnetic field and spin torques which result in an oscillation of resistance due to the GMR effect. A homodyne mixture of rf current and oscillatory resistance produces a large dc voltage at the resonance of the free layer [Fig. 1(d)] [13,23,32]. Since we have a dominant GMR effect, we expect the maximum dc voltage signal when the angle between the free and fixed

layers is 90° , and the signal should vanish when the free and pinned layers are parallel or antiparallel (see Appendixes A and B).

The dc voltage measured by the STFMR technique [Figs. 1(d), 2, and 3] can be fitted to a sum of symmetric Lorentzian (V_S) and antisymmetric Lorentzian (V_A) functions:

$$V_S = C_1 \frac{\Delta^2}{4(f - f_0)^2 + \Delta^2}, \quad V_A = C_2 \frac{4(f - f_0)\Delta}{4(f - f_0)^2 + \Delta^2},$$

where f_0 is the resonance frequency, C_1 and C_2 are the peak amplitudes of voltages corresponding to V_S and V_A , respectively, and Δ represents the linewidth (FWHM). f_0 as a function of the applied magnetic field can be fitted to following Kittel's formula as shown in the inset in Fig. 1(d): $f_0 = (\gamma/2\pi)\sqrt{(H_P + H_{\text{ext}})[(H_P + H_{\text{ext}} + H_\perp)]}$, where H_P is an in-plane anisotropy field (approximately 50 Oe), H_\perp is an out-of-plane anisotropy field (approximately 1.35×10^4 Oe), H_{ext} is an external applied magnetic field, and γ is the gyromagnetic ratio (2.05×10^5 A/m sec). The antisymmetric component (V_A) of dc voltage arises from an in-plane field Oersted magnetic field. The symmetric Lorentzian (V_S) component can arise from two different ways: (i) an in-plane polarized spin current (generated by the AHE of the fixed layer and injected to the free magnet) and (ii) an out-of-plane magnetic field (generated by the in-plane current). The coordinate frame used for the analysis is shown in Fig. 1(c). Let us consider that the sample is in the X-Y plane, the rf current flows along the X axis, and the dc voltage is also measured along the X axis [Fig. 1(c)]. The equilibrium magnetization direction of the free layer (m) and the pinned layer (M) is in the X-Y plane and makes angles of θ_m and θ_M with respect

to the X axis. In the following sections, we show the experimental evidence which indicates that the in-plane current-induced out-of-plane field (\mathbf{H}_{eff}) has a dominant role in spin torque in this GMR device where $\mathbf{H}_{\text{eff}} = \beta_{\text{pseudo}}(\mathbf{M} \times \mathbf{J})$ (\mathbf{J} is the current density, and β_{pseudo} is a constant).

IV. EXPERIMENTAL RESULTS

Figures 2(a)–2(g) show a detailed study of STFMR for different configurations. Figures 2(a) and 2(b) show the results when an external field of 450 Oe is applied along the $+X$ and $-X$ directions, respectively, while the fixed-layer magnetization is along the $-Y$ direction ($\theta_M = -90^\circ$). The black curve denotes experimental data after subtracting the background voltage. The dc voltage with both free- and pinned-layer magnetizations along the X axis is taken as background [see Fig. 6(h) in Appendix C]. The fitted red curve is the sum of a symmetric Lorentzian (V_S ; blue curve) and an antisymmetric Lorentzian (V_A , green curve). Both cases in Figs. 2(a) and 2(b) show that the sign of V_A is the same, whereas V_S changes sign when the external field is reversed. The relative sign change between the V_S and V_A components is rather surprising, and this point can be appreciated by comparing results of a standard STFMR experiment [26,30,31] on a NM-FM sample [see Figs. 6(c)–6(d) in Appendix C].

In the STFMR experiment, the generated dc voltage is proportional to the product of $dR/d\theta_m$ (derivative of sample resistance) and “efficiency of excitation.” The efficiency of excitation is defined by the component of excitation perpendicular to the equilibrium magnetization of the free layer [10]. Thus, the efficiency of spin current generated by the SHE (or AHE) and an Oersted magnetic field is $\cos \theta_m$. Efficiency zero implies no torque on free-layer magnetization. If the current generates an out-of-plane magnetic field along the Z axis, its efficiency is one, as it is always

perpendicular to the equilibrium magnetization which is in the X - Y plane. Refer to Appendix A for a detailed discussion.

V. ORIGIN OF DIFFERENT TORQUES

In the case of a GMR sample, the resistance is proportional to $\cos(\theta_M - \theta_m)$, where $(\theta_M - \theta_m)$ is the angle between the free and fixed layers. If the pinned layer is along the $-Y$ direction, i.e., $\theta_M = -90^\circ$, the derivative of sample resistance is proportional to $-\cos \theta_m$. Thus, in this configuration ($\theta_M = -90^\circ$), dc voltage produced by an Oersted magnetic field or the SHE has $\cos^2 \theta_m$ angular dependence, whereas dc voltage produced by an out-of-plane magnetic field has $\cos \theta_m$ angular dependence. It means that, upon external magnetic-field reversal (i.e., $\theta_m \rightarrow 180^\circ + \theta_m$), the dc voltage produced by an Oersted field or a spin current (generated by the SHE or AHE) remains the same, whereas dc voltage produced by an out-of-plane magnetic field changes sign. Furthermore, it can be shown that the dc voltage spectrum arising from an Oersted magnetic field has an anti-Lorentzian shape, whereas the dc voltage spectrum arising from the SHE or AHE or an out-of-plane magnetic field has a Lorentzian shape. This is related to the susceptibility of the X component of magnetization to oscillating magnetic fields along the Y or Z directions and an oscillating spin current polarized along the Y direction (see Appendix A for details). This implies that, from the data shown in Figs. 2(a) and 2(b), the antisymmetric Lorentzian component of the dc voltage of a GMR sample can be ascribed to the Oersted magnetic field, as it remains the same upon external magnetic-field reversal. It is also intuitive that most of the current flows below the free layer, creating a large Oersted field (22 nm of different metals are below the free layer, whereas a 5-nm Cu film is on top of the free layer; see Appendix B). On the other hand, the symmetric component

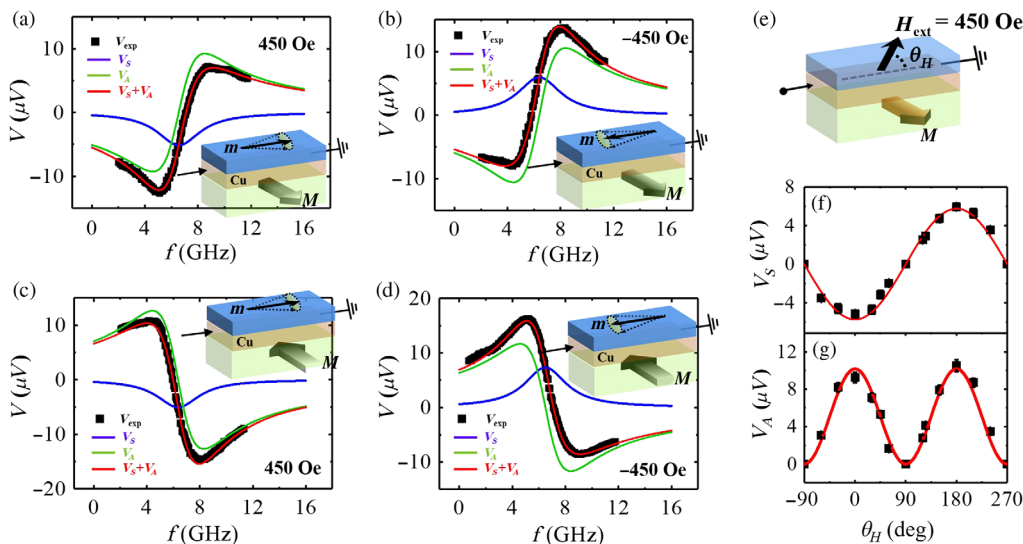


FIG. 2. STFMR experiment of a current in-plane GMR sample for different configurations: (a) $\theta_M = -90^\circ$, $\theta_m = 0^\circ$. (b) $\theta_M = -90^\circ$, $\theta_m = 180^\circ$. (c) $\theta_M = +90^\circ$, $\theta_m = 0^\circ$. (d) $\theta_M = +90^\circ$, $\theta_m = 180^\circ$. (e)–(g) Detailed angular dependence of V_S and V_A .

can be ascribed to the out-of-plane magnetic field, as it changes sign upon external magnetic-field reversal and it has a Lorentzian shape. Hence, it is evident that the out-of-plane field has completely dominated the spin-current-induced torque owing to the AHE of the FM. The existence of such an anomalous magnetic field in a GMR sample is a unique observation.

Such an out-of-plane magnetic field can be obtained by the following combinations: (i) $\mathbf{m} \times \mathbf{M}$, (ii) $\mathbf{m} \times \mathbf{J}$, and (iii) $\mathbf{M} \times \mathbf{J}$. The first two combinations imply that the magnetic field is along the Z axis but changes sign if \mathbf{m} inverts; i.e., the efficiency of the excitation changes sign. This implies that the dc voltage arising from these terms does not invert when \mathbf{m} inverts and therefore cannot explain the symmetric Lorentzian term in Figs. 2(a) and 2(b). The combination $(\mathbf{M} \times \mathbf{J})$ creates a magnetic field along the Z axis independent of the orientation of \mathbf{m} , and, thus, the symmetric Lorentzian component observed in the dc voltage of the GMR sample can be ascribed to a current-induced out-of-plane magnetic field of the form $\mathbf{H}_{\text{eff}} = \beta_{\text{pseudo}}(\mathbf{M} \times \mathbf{J})$. The magnetic field (\mathbf{H}_{eff}) and magnetization (\mathbf{M}) are axial (pseudo) vectors, whereas the current density (\mathbf{J}) is a polar vector. As the cross product $(\mathbf{M} \times \mathbf{J})$ is a polar vector, the constant β_{pseudo} must be a pseudoscalar so that the right-hand side of the above expression is a pseudovector. More discussion about the necessity of a pseudoscalar to explain the experimental data on the GMR sample is provided in Appendix D.

VI. ANALYSIS

We now analyze the data shown in Figs. 2(c) and 2(d). Figures 2(a) and 2(c) show that V_S remains the same but V_A changes sign. Going from the configuration shown in Figs. 2(a)–2(c), derivative of sample resistance ($dR/d\theta_m$) and the effective out-of-plane magnetic field (hence the efficiency of excitation), both change sign as the fixed-layer magnetization is inverted. So V_S remains the same as it originates from the out-of-plane field. On the other hand, the Oersted magnetic field created by the current (and associated efficiency of excitation) remains unchanged as it does not depend on \mathbf{M} . So V_A changes sign due to the sign change of $dR/d\theta_m$ [compare Figs. 2(a) and 2(c)]. This also further supports that V_A originates from an Oersted field. The same conclusion can be made by comparing Figs. 2(b) and 2(d). Starting from the configuration shown in Fig. 2(a),

we can reach the configuration shown in Fig. 2(d) by rotating the X - Y axes 180° about the Z axis. As the voltage-measuring terminals are not rotated, the entire dc voltage signals in Figs. 2(a) and 2(d) have opposite signs, which is consistent with symmetry arguments (see Appendix D for the detailed symmetry analysis). Furthermore, we perform a detailed analysis of the angular dependence of dc voltage after fitting it with V_S and V_A as shown in Figs. 2(f) and 2(g). It is clearly seen that the angular dependence of V_S and V_A shows close to $\cos \theta_m$ and $\cos^2 \theta_m$ dependence, respectively, which is quite consistent with the above discussion (see Appendixes A–C for a detailed discussion).

VII. SPECIAL CASE STUDIES

From the expression of anomalous field $\mathbf{H}_{\text{eff}} = \beta_{\text{pseudo}}(\mathbf{M} \times \mathbf{J})$, it follows that, if the current flows along the pinned-layer magnetization, there should not be any out-of-plane magnetic field, and hence V_S in the dc voltage should vanish. We test this experimentally, and results are shown in Fig. 3(a), which shows that V_S is very small compared to V_A . We can also have another interesting configuration where the dc voltage contains only the V_S term but no V_A . Such a configuration is shown in Fig. 3(b), where the pinned layer makes a 45° angle with the X axis and free-layer magnetization is along the Y axis. In this case, the Oersted magnetic field is parallel to the equilibrium magnetization direction of the free layer. Hence, it does not excite FMR, whereas the anomalous magnetic field along the Z axis is nonzero and excites FMR. From Fig. 3(b), we can see that V_A is very small compared to V_S . These results strongly support the existence of an anomalous in-plane current-driven out-of-plane magnetic field in the GMR sample. A third special case is where both V_A and V_S should vanish, in principle, when fixed-layer magnetization is parallel to the current flow (X axis) and free-layer magnetization points perpendicular to this (Y axis) as shown in Fig. 3(c). In this case, though the GMR detection is active, as both the Oersted magnetic field and anomalous magnetic field fail to excite FMR, no dc voltage is expected. An experimentally measured dc voltage signal is also fairly small compared to Fig. 2. A small but nonzero signal is observed due to the tilting of the fixed layer when an external field is perpendicular to it. While 450 Oe is applied perpendicular to the pinned layer, it can tilt approximately 16° considering its exchange bias to be

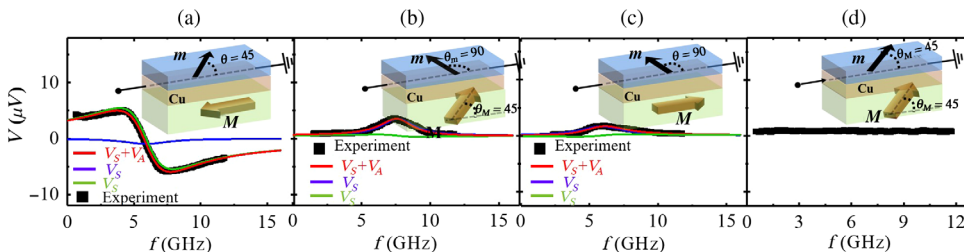


FIG. 3. Special case studies. (a) $\theta_M = 180^\circ$, $\theta_m = 45^\circ$. (b) $\theta_M = 45^\circ$, $\theta_m = 90^\circ$. (c) $\theta_M = 0^\circ$, $\theta_m = 90^\circ$. (d) $\theta_M = \theta_m = 45^\circ$. The applied external magnetic field is 400 Oe in all these experiments.

1.6 kOe, which can explain the appearance of such a small signal in Fig. 3(c) (see Appendixes B and C for more details). In a control experiment where the fixed layer and free layer are parallel ($\theta_M = 45^\circ$, $\theta_m = 45^\circ$), we do not observe any STFM signal [Fig. 3(d)]. This shows that our detection method is based on resistance variation due to the current in-plane GMR effect [Fig. 1(b)]. All these measurements support the form of anomalous field we propose.

VIII. DISCUSSION

Recently, it was predicted that, in a GMR kind of structure, a fixed layer can produce torque on a free layer owing to the anomalous Hall effect and AMR of the FM [28]. But, this AMR effect is not expected to produce spin torque with an in-plane fixed layer. In a GMR kind of structure, the fixed layer and free layer are not decoupled from each other, as far as in-plane current flow is present. Scattering and reflection of spins take place at the interface through the Cu spacer due to the zigzag motion of carriers which causes the in-plane GMR effect. So we cannot think of a simple picture of a GMR stack where current flows in parallel channels through the fixed layer, free layer, and Cu spacer unlike HM-FM bilayers. If the fixed FM behaves similar to other heavy metals (Pt, Ta, W, etc.), we would expect an injection of spin current from a fixed FM to a free FM through the spin transport via the Cu spacer. In that situation, we would not see a sign reversal of the symmetric component while reversing the external magnetic field as observed here (Fig. 2). It is possible that the current in-plane GMR effect (interfacial spin scattering and zigzag motion of electrons between fixed and free layers through the Cu spacer) in combination with spin-orbit coupling could produce such an in-plane current-induced out-of-plane effective magnetic field which exerts torque on the free layer. Even for that, we have to break the mirror symmetry of the lateral dimension. Previously, this kind of out-of-plane magnetic field was reported in a wedge-shaped Ta/CoFeB/TaO_x heterostructure [15]. It is possible that after performing magnetic annealing different layers become crystalline and chirality or strain may be induced in the device, which breaks the mirror symmetry of the GMR device [36]. We furthermore cannot rule out the possibility of noncollinearity of magnetic domains inside the device, which can also create such an anomalous field. Our proposed expression of such an out-of-plane effective field can explain the experimentally observed data, but further theoretical study is required to understand the microscopic origin of this anomalous field in a GMR structure. We estimate that an approximately 125-Oe effective out-of-plane magnetic field is created when average 10^{12} A/m² current density flows in a FM (free = 2 nm)/Cu(5 nm)/FM (fixed = 2 nm) heterostructure (see Appendix C for the calculation).

IX. CONCLUSION

In summary, we report a unique observation of an in-plane current-induced out-of-plane magnetic field in a GMR structure. Our experiment suggests the possibility of crystalline chirality or strain, which may occur during the fabrication steps, generating such anomalous spin torques. It would be interesting to engineer crystal structures controllably which can allow forms of spin torques which are generally prohibited in conventional structures. Another advantage is that this spin-orbit torque by a ferromagnet can be tuned by the magnetization of a fixed layer. The generation of such an out-of-plane field will be of interest for switching applications of perpendicular magnetic bits.

ACKNOWLEDGMENTS

We are thankful to the Centre of Excellence in Nanoelectronics (CEN) at the IIT-Bombay Nanofabrication facility (IITBNF) and the Ministry of Electronics and Information Technology (MeitY), Government of India, for the support. A. B. played a primary role to plan the work with A. T. The GMR stack was deposited by D. D. L. and Y. J. with the supervision of S. M. and M. G. A. B. prepared the sample, performed the measurement, and analyzed the data with the help of S. B., H. S., and S. D. A. T. provided the expression of the anomalous spin torque and theoretical calculations. A. T. supervised the project.

Note added.—Recently, the authors came to know the reports of spin-orbit torque by the anomalous Hall effect in a spin-valve structure in Refs. [37,38]. In these papers, the bottom FM is not pinned, and also the anomalous magnetic-field term is not observed.

APPENDIX A: DERIVATION OF THE EXPRESSION FOR THE dc VOLTAGE

The reference frame used is shown below (Fig. 4).

The green rectangle denotes the GMR stack cut into rectangular shape. The rf current flows along the X axis. The equilibrium free-layer and pinned-layer magnetization directions (\hat{m} and \hat{m}_{pin}) are assumed to be in the X - Y plane. The X' axis is taken to be along \hat{m} . When the current is passed along the X direction, it creates an Oersted magnetic field along the y axis, $\bar{h} = h_{\text{Oe}}\hat{y}$. The anomalous magnetic field is given by $\bar{h}_{\text{new}} = \beta(\hat{m}_{\text{pin}} \times \bar{J}) = -\beta J m_{\text{pin},y} \hat{z}$, where β is a constant and $m_{\text{pin},y}$ denotes the Y component

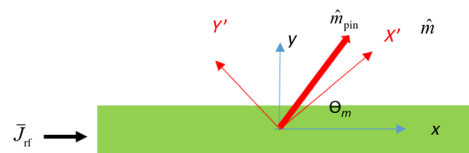


FIG. 4. Estimation of STFM voltage.

of \hat{m}_{pin} . Assuming a small oscillation of \hat{m} , we get the following equations:

$$\delta m_{y'} = \chi_{11} h_{y'} + \chi_{12} h_z = \chi_{11} h_{\text{Oe}} \cos \theta_m - \beta J m_{\text{pin},y} \chi_{12}, \quad (\text{A1})$$

$$\begin{aligned} \Rightarrow \delta m_x &= -\sin \theta_m \delta m_{y'} \\ &= (-\sin \theta_m \cos \theta_m \chi_{11} h_{\text{Oe}} + \sin \theta_m \beta J m_{\text{pin},y} \chi_{12}), \end{aligned} \quad (\text{A2})$$

$$\begin{aligned} \text{and } \delta m_y &= \cos \theta_m \delta m_{y'} \\ &= (\cos^2 \theta_m \chi_{11} h_{\text{Oe}} - \cos \theta_m \beta J m_{\text{pin},y} \chi_{12}), \end{aligned} \quad (\text{A3})$$

where χ denotes the magnetic susceptibility tensor.

The sample resistance depends on the relative orientation of \hat{m} and \hat{m}_{pin} and undergoes an oscillation if \hat{m} oscillates, as follows:

$$\begin{aligned} R &= R_P + \frac{\Delta R}{2} (1 - \hat{m} \cdot \hat{m}_{\text{pin}}) \\ \Rightarrow \delta R &= -\frac{\Delta R}{2} (m_{\text{pin},x} \delta m_x + m_{\text{pin},y} \delta m_y). \end{aligned} \quad (\text{A4})$$

The homodyne mixture of the oscillating current and resistance produces a dc voltage given by

$$\begin{aligned} V_{\text{dc}} &= \frac{1}{2} I_{\text{rf}} \text{Re}(\delta R) \\ &= \frac{-1}{4} I_{\text{rf}} \Delta R [m_{\text{pin},x} \text{Re}(\delta m_x) + m_{\text{pin},y} \text{Re}(\delta m_y)]. \end{aligned} \quad (\text{A5})$$

From the above equations, we see that the Oersted magnetic-field term is multiplied by $\text{Re}(\chi_{11})$, which has a dispersion shape, whereas the anomalous magnetic-field term is multiplied by $\text{Re}(\chi_{12})$, which shows a peak at resonance.

Let us now see how the dc voltage changes when we reverse \hat{m} and/or \hat{m}_{pin} . If we reverse \hat{m} , keeping \hat{m}_{pin} the same (i.e., $\theta_m \rightarrow \theta_m + \pi$), the Oersted magnetic-field term

remains the same as it involves factors of $\sin \theta_m \times \cos \theta_m$ and $\cos^2 \theta_m$, whereas the anomalous magnetic-field-driven term inverts as it involves factors of $\sin \theta_m$ and $\cos \theta_m$. If we reverse \hat{m}_{pin} , keeping \hat{m} the same, we see from Eq. (A5) that V_{dc} gets a minus sign. However, the anomalous magnetic-field term itself changes sign if we invert \hat{m}_{pin} . Thus, the Oersted magnetic-field term changes sign, whereas the anomalous magnetic-field term remains the same in this case. Combining the above two scenarios, if we reverse both \hat{m} and \hat{m}_{pin} , both the terms change sign; i.e., the dc voltage inverts. These conclusions are in agreement with the experimental data shown in Figs. 3(a)–3(d).

If the free and pinned layers are parallel (i.e., $m_{\text{pin},x} = \cos \theta_m$ and $m_{\text{pin},y} = \sin \theta_m$), the dc voltage is 0 as can be seen from Eqs. (A2), (A3), and (A5).

We now take a particular case where the pinned layer is along the y axis. From Eqs. (A3) and (A5), the dc voltage is given by

$$\begin{aligned} V_{\text{dc}} &= \frac{-1}{4} I_{\text{rf}} \Delta R \text{Re}(\delta m_y) \\ &= \frac{-1}{4} I_{\text{rf}} \Delta R [\cos^2 \theta_m \text{Re}(\chi_{11}) h_{\text{Oe}} - \cos \theta_m \beta \text{Re}(\chi_{12}) J]. \end{aligned} \quad (\text{A6})$$

The above equation shows that the antisymmetric Lorentzian (dispersion) term has $\cos^2 \theta_m$ dependence whereas the symmetric Lorentzian term has $\cos \theta_m$ dependence in agreement with the experimental data in Figs. 3(c) and 3(d).

APPENDIX B: ESTIMATION OF MAGNETIZATION ANGLE BETWEEN FREE AND FIXED LAYERS AND ITS IMPACT ON STFMR

In the STFMR experiment, we have swept frequency for a particular external dc magnetic field which is in the range of 400–500 Oe. The coercivity of the free layer is around 40 Oe. Hence, the free layer almost aligns to the external magnetic field. For example, at 450 Oe, the estimated

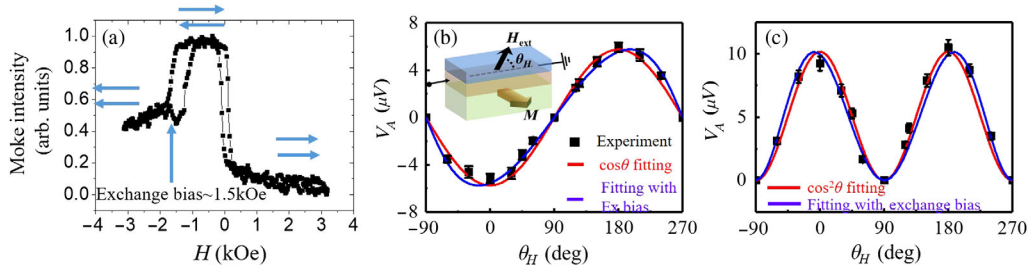


FIG. 5. (a) Magneto-optic Kerr measurement of the GMR stack. (b),(c) Angular dependence of symmetric (V_S) and antisymmetric (V_A) component of the STFMR experiment, respectively. The red curve in (b) and (c) indicates $\cos \theta$ and $\cos^2 \theta$ dependence, respectively. The blue curve in (b) and (c) is obtained numerically by taking into account the rotation of the fixed layer due to finite exchange bias (approximately 1.6 kOe).

maximum difference in between the free layer and external magnetic-field directions is less than 2.5° . The magnetization direction of the fixed layer can change a bit when an external magnetic field is applied, which can be estimated from the pinning strength. The magnetization of the stack measured by Kerr rotation [Fig. 5(a)] indicates that the pinning-field strength is about 1.6 kOe. The angular dependence of the symmetric and antisymmetric components of the dc voltage shown in Figs. 2(f) and 2(g) [and Figs. 5(b) and 5(c)] would show some deviation from $\cos \theta_m$ and $\cos^2 \theta_m$ dependence if the fixed layer moves. We numerically evaluate the angular dependence, taking into account the rotation of the fixed layer which is shown by the blue curve in Figs. 5(b) and 5(c). The red curve shows $\cos \theta_m$ and $\cos^2 \theta_m$ dependence. The experimental results (black data points) are well described by the blue curve.

APPENDIX C: NUMERICAL EVALUATION OF THE dc VOLTAGE SIGNAL AND ADDITIONAL EXPERIMENTAL DATA

We can numerically evaluate the dc voltage from the equation provided in Appendix A. The Oersted magnetic field depends on the current distribution in the sample, which can be obtained from the electrical conductivities of the various layers in the stack. The anomalous magnetic field is given by $\vec{h} = \beta(\hat{m}_{\text{pin}} \times \vec{J})$, where J is taken as the average current density flowing in the free layer/Cu spacer/pinned layer stack and β is taken as a parameter to be evaluated. We assume a uniform current density, a uniform Oersted magnetic field, and uniform magnetizations in the analysis.

The following parameters are used for numerical calculation.

Metal	Thickness (nm)	Resistivity (Ωm)
Cu (cap)	3	8×10^{-8}
CoFe (free layer)	2	2.7×10^{-7}
Cu (spacer)	5	8×10^{-8}
CoFeB (pinned)	2	2.7×10^{-7}
Buffer layer [IrMn(7) + R(5) + Ta(5)]	17	2.5×10^{-7} (equivalent)

The length (L_x) of the GMR sample is $375 \mu\text{m}$, and the width is $25 \mu\text{m}$. The applied field is 450 Oe. Our GMR sample shows a high out-of-plane anisotropic field (approximately 13.5 kOe) and higher damping ($\alpha \sim 0.09$). The chosen resistivity closely matches the experimental and simulated resistance of the GMR stack and magnetoresistance. The experimentally obtained resistance of the in-plane GMR stack is around 88Ω , whereas the simulated result of GMR resistance is 85.5Ω . The rotation of the fixed layer on application of an external magnetic field is also taken into account in the numerical calculation. It is found that $\beta \approx -10^{-8} \text{ m}$ gives a reasonable match to the experimental data as shown in Figs. 6(a) and 6(b) for two different configurations. This value can be written as $\beta \approx 125 \text{ Oe}/10^{12} (\text{A}/\text{m}^2)$; i.e., an average current density of $10^{12} \text{ A}/\text{m}^2$ passing through CoFe(2 nm)/Cu(5 nm)/CoFe(2 nm) layers produces a magnetic field of 125 Oe along the Z direction on the free layer if the pinned layer and current are perpendicular to each other.

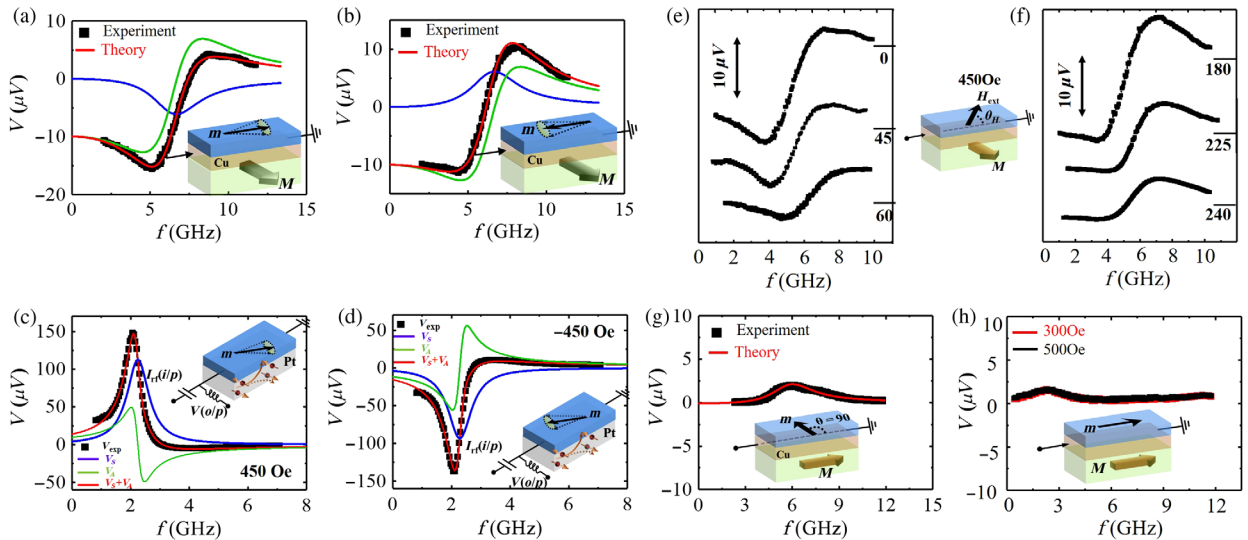


FIG. 6. (a),(b),(e)–(h) STFM spectrum of a GMR sample for different configurations described in the inset in the figures. (c),(d) STFM spectrum for a Pt/Ni sample. (e),(f) Angular dependence of STFM of a GMR stack. (h) Background data when free and fixed layers are parallel for a 300- (red) and 500-Oe (black) applied field. Red curves in (a)–(d) and (f),(g) represent numerically estimated voltage, whereas black curves show experimental data.

Figures 6(a), 6(b), and 6(g) show the experimental data fitted with Eq. (A6) solving it analytically. This is in good agreement with the fitting of these experimental results with symmetric Lorentzian (V_S) and antisymmetric Lorentzian (V_A) components as shown in Figs. 2(a), 2(b), and 3(c). In Fig. 6(g) [or Fig. 3(c)], the expected dc voltage is zero if we assume that the pinned layer does not rotate, i.e., remains along the X axis, when a magnetic field along the Y axis is applied. Experimentally, we do observe a small dc voltage [compare Figs. 6(a) and 6(g)] in this configuration, which can be explained by the rotation of the fixed layer as argued in Appendix B. The numerical calculation [red curve in Fig. 6(g)] considering a 1.6-kOe exchange bias can reproduce the experimental data as shown in Fig. 6(g). Figure 6(h) shows the experimental data when both free and pinned layers are along the X axis (parallel to current) for two different values of the external magnetic field (300 and 500 Oe). In both these cases, we see no signal from STFMR, since our detection method is based on the in-plane GMR effect. However, at a low frequency range (around 1–2 GHz), a small peak (amplitude less than $1.5 \mu\text{V}$) appears (in all the cases) which are magnetic field independent [Fig. 6(h)]. This is considered as background voltage which is subtracted from all the experimental data presented in the main article. Typically, resonance frequencies in our experiment are the range of 5–6 GHz, which allows us to detect a STFMR signal with minimal error. Figures 6(e) and 6(f) show an angular dependence of the STFMR spectrum of the GMR stack as shown in the schematic representation. V_S and V_A corresponding to Figs. 6(e) and 6(f) are shown in Figs. 2(e) and 2(f) in the main text.

One important point to note is that, on reversal of the magnetic field, the sign of STFMR voltage for a GMR stack is inverted such that there is a relative change in sign between V_S and V_A . This kind of relative change of sign between V_S and V_A is not expected if dc voltage is produced by an Oersted field or spin current. We can verify this by comparing STFMR of Ni/Pt bilayers [Figs. 6(c) and 6(d)], which is standard and very well known. It is clearly seen that, when the magnetic-field polarity is changed ($45^\circ \rightarrow 225^\circ$), the sign of the entire dc voltage is inverted, which means both V_S and V_A components change sign. So there is no relative sign change between V_S and V_A in Ni/Pt samples as compared to these GMR samples [Figs. 6(a)–6(d)]. Recall that V_S and V_A in the Ni/Pt sample arise from spin current due to the spin Hall effect and Oersted field, respectively. In this regard, STFMR data in the GMR sample are unique, which can be explained by an out-of-plane effective field as mentioned in the previous section.

APPENDIX D: TRANSFORMATION PROPERTIES OF β_{pseudo}

Let us consider a situation when free-layer magnetization (\mathbf{m}) is along the X axis, pinned-layer magnetization (\mathbf{M})

along the $-Y$ axis, and current flow along the X axis [Fig. 7(a)]. If we take its mirror reflection with respect to the ZX plane, we get the situation as shown in Fig. 7(b) (same configuration as Fig. 2(b)). The reflection from Fig. 7(a) to Fig. 7(b) indicates that \mathbf{m} inverts (as magnetization is a pseudovector) and \mathbf{M} , \mathbf{J} , and \mathbf{E}_{dc} remain the same. So, we expect that there should not be any change in dc voltage upon the reflection with respect to the ZX plane. We see that the antisymmetric spectrum (V_A , Oersted magnetic-field component) did not change sign and behaves conventionally. However, the sign of the symmetric spectrum (V_S) is inverted. This implies that the mirror reflection symmetry of the sample is broken, which manifests as a pseudoscalar in the description of the V_S component. The pseudoscalar changes sign on mirror reflection, which inverts the sign of V_S .

Similarly, if we take the mirror reflection of Fig. 7(a) with respect to the YZ plane, we get the situation as shown in Fig. 7(c). From Fig. 7(a) to Fig. 7(c), there is a change in sign of \mathbf{M} and \mathbf{E} , but \mathbf{m} remains the same as magnetization is a pseudovector. So, the measured voltage should change its sign while reflection is taken with respect to the YZ plane. Figure 7(c) shows the same configuration corresponding to the data shown in Fig. 2(c) with the difference that the current flow is along the $-X$ direction. It is to be noted that the dc voltage is proportional to the power of the rf current (I^2). Hence, the phase of current does not influence the dc voltage signal; i.e., ac current along the $\pm X$ direction gives the same dc voltage. It is evident that the V_A term in Fig. 7(c) [and hence Fig. 2(c)] is inverted with respect to Fig. 7(a) [and Fig. 2(a)] unlike the V_S term [compare V_S in Figs. 7(a) and 7(c)]. This again shows that the Oersted term follows the mirror reflection symmetry; i.e., it changes sign as the mirror image of \mathbf{E}_{dc} changes sign. The symmetric component V_S , on the other hand, remains the same again, which implies that a pseudoscalar is needed to describe it.

The fact that the electric field or dc voltage inverts in Fig. 7(c) can also be concluded from the following argument: If we take the mirror reflection of the oscillating \mathbf{m} in Fig. 7(a), there is a 180° phase shift in the reflected image in Fig. 7(c). This is because upon mirror reflection $m_x \rightarrow m_x$, $m_y \rightarrow -m_y$, and $m_z \rightarrow -m_z$. However, since the pinned-layer magnetization is also opposite for these two cases, and as resistance depends on the dot product $\mathbf{m} \cdot \mathbf{M}$, the oscillating resistance is the same in both the cases at each instant of time. However, as the current is opposite, the dc voltage is opposite.

Now the reflection of Fig. 7(c) along the ZX plane [or reflection of Fig. 7(b) along the YZ plane] gives the situation of Fig. 7(d), which is the same situation shown in Fig. 2(d). This is also consistent with the previous arguments of reflection; i.e., V_A follows regular symmetry and V_S follows the expected symmetry considering a pseudoscalar to describe it. Another important point is

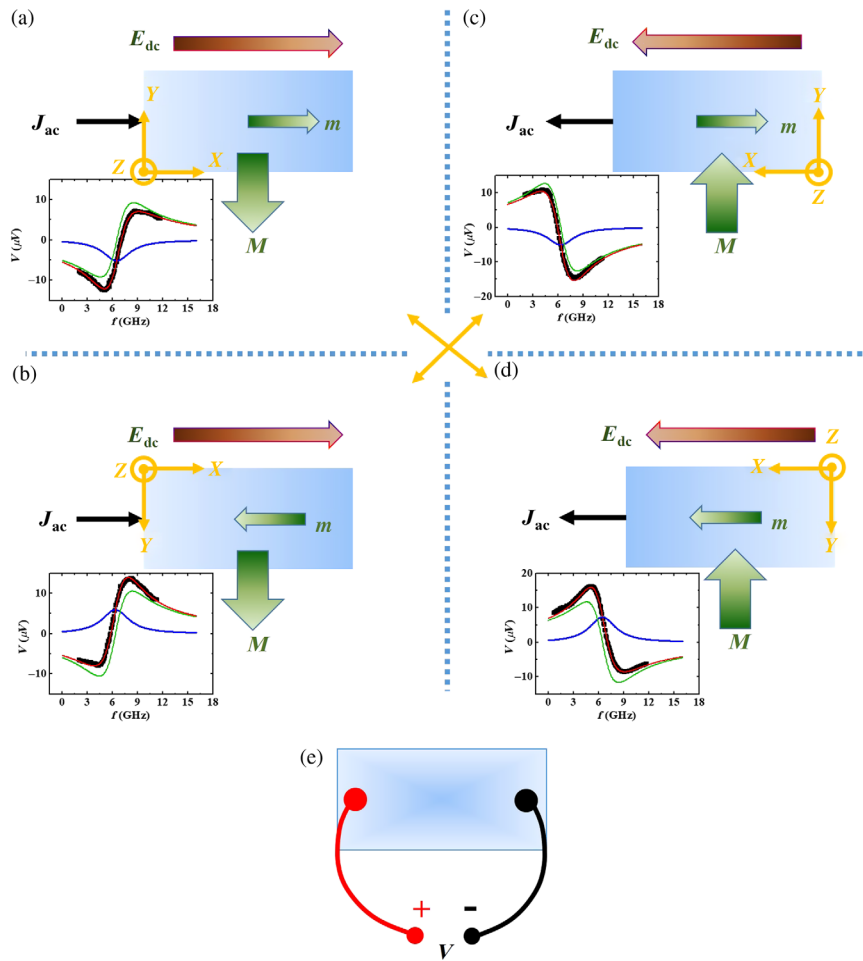


FIG. 7. Symmetry analysis of the voltage signal. Schematics of the device with a free magnet (m), fixed magnet (M), and current density (J) are shown with a mirror reflection corresponding to experiments [Figs. 2(a)–2(d)] in the same panel. Data shown in (a) and (c) are related to the mirror reflection through the ZX plane. V_A (Oersted field component) did not change its sign, but the sign of V_S is changed, which requires pseudoscalar operation (the same for all other cases). Two times mirror reflection of (a) is the same as (d), which is also the same as in-plane 180° sample rotation (it is also indicated with a yellow arrow at the center). (e) shows the voltage terminals of the device. The voltage is proportional to the power of the applied rf current, and hence the polarity of the rf current does not matter. Mirror reflection from (a) to (c) [or (b) to (d)] causes the interchange of voltage terminals. But in the actual experiment voltage terminals were fixed as shown in (e).

that the configuration shown in Fig. 7(d) can be achieved by rotating the frame shown in Fig. 7(a) by 180° in which both V_S and V_A are expected to be changed and the same thing also observed experimentally. A 180° in-plane rotation involves two times mirror reflections, which does not change the sign of the pseudoscalar.

Previous symmetry arguments suggest that we should have a pseudoscalar behind the origin of V_S . Earlier, we argued that our observed results can be explained by assuming an anomalous magnetic field of the form

$$\vec{H} = \beta_{\text{pseudo}}(\hat{M} \times \vec{J}).$$

\vec{H} (effective magnetic field) and \hat{M} (pinned magnetization direction) in the above equation are axial (pseudo) vectors, whereas \vec{J} is a polar vector. As $(\hat{M} \times \vec{J})$ is a polar vector, β_{pseudo} must be a pseudoscalar so that the right-hand side of the above equation transforms like an axial vector, i.e., the same as the left-hand side. Similarly, since \vec{H} , \hat{M} , and \vec{J} are odd under time reversal, β_{pseudo} should also be odd under time reversal. The existence of a pseudoscalar requires the broken mirror symmetry of the GMR stack. (This situation

can be compared to the magnetoelectric effect, where application of an electric field results in magnetization: $\vec{M} = \kappa \vec{E}$. The pseudoscalar κ is nonzero only if the crystal lacks mirror symmetry.)

-
- [1] J. Sinova, S. O. Valenzuela, J. Wunderlich, C. H. Back, and T. Jungwirth, Spin Hall effects, *Rev. Mod. Phys.* **87**, 1213 (2015).
 - [2] A. Brataas, Y. Tserkovnyak, G. E. W. Bauer, and B. I. Halperin, Spin battery operated by ferromagnetic resonance, *Phys. Rev. B* **66**, 060404(R) (2002).
 - [3] K. I. Uchida, H. Adachi, T. Ota, H. Nakayama, S. Maekawa, and E. Saitoh, Observation of longitudinal spin-Seebeck effect in magnetic insulators, *Appl. Phys. Lett.* **97**, 172505 (2010).
 - [4] G. E. W. Bauer, E. Saitoh, and B. J. Van Wees, Spin caloritronics, *Nat. Mater.* **11**, 391 (2012).
 - [5] A. Bose, S. Bhuktare, H. Singh, V. G. Achanta, and A. A. Tulapurkar, Direct detection of spin Nernst effect in platinum, *Appl. Phys. Lett.* **112**, 162401 (2018).
 - [6] A. Manchon, H. C. Koo, J. Nitta, S. M. Frolov, and R. A. Duine, New perspectives for Rashba spin-orbit coupling, *Nat. Mater.* **14**, 871 (2015).

- [7] I. M. Miron, G. Gaudin, S. Auffret, B. Rodmacq, A. Schuhl, S. Pizzini, J. Vogel, and P. Gambardella, Current-driven spin torque induced by the Rashba effect in a ferromagnetic metal layer, *Nat. Mater.* **9**, 230 (2010).
- [8] A. Chernyshov, M. Overby, X. Liu, J. K. Furdyna, Y. Lyanda-Geller, and L. P. Rokhinson, *Nat. Phys.* **5**, 656 (2009).
- [9] S. Bhuktare, A. Bose, H. Singh, and A. A. Tulapurkar, Gyration based on magneto-elastic coupling at a ferromagnetic/piezoelectric interface, *Sci. Rep.* **7**, 840 (2017).
- [10] A. Brataas, A. D. Kent, and H. Ohno, Current-induced torques in magnetic materials, *Nat. Mater.* **11**, 372 (2012).
- [11] I. M. Miron, K. Garello, G. Gaudin, P. J. Zermatten, M. V. Costache, S. Auffret, S. Bandiera, B. Rodmacq, A. Schuhl, and P. Gambardella, Perpendicular switching of a single ferromagnetic layer induced by in-plane current injection, *Nature (London)* **476**, 189 (2011).
- [12] L. Liu, C.-F. Pai, Y. Li, H. W. Tseng, D. C. Ralph, and R. A. Buhrman, Spin-torque switching with the giant spin Hall effect of tantalum, *Science* **336**, 555 (2012).
- [13] L. Liu, T. Moriyama, D. C. Ralph, and R. A. Buhrman, Spin-Torque Ferromagnetic Resonance Induced by the Spin Hall Effect, *Phys. Rev. Lett.* **106**, 036601 (2011).
- [14] D. Fang, H. Kurebayashi, J. Wunderlich, K. Výborný, L. P. Žárbo, R. P. Campion, A. Casiraghi, B. L. Gallagher, T. Jungwirth, and A. J. Ferguson, Spin-orbit-driven ferromagnetic resonance, *Nat. Nanotechnol.* **6**, 413 (2011).
- [15] G. Yu, P. Upadhyaya, Y. Fan, J. G. Alzate, W. Jiang, K. L. Wong, S. Takei, S. A. Bender, L. Te Chang, Y. Jiang, M. Lang, J. Tang, Y. Wang, Y. Tserkovnyak, P. K. Amiri, and K. L. Wang, Switching of perpendicular magnetization by spin-orbit torques in the absence of external magnetic fields, *Nat. Nanotechnol.* **9**, 548 (2014).
- [16] A. Bose, A. K. Shukla, K. Konishi, S. Jain, N. Asam, S. Bhuktare, H. Singh, D. D. Lam, Y. Fujii, S. Miwa, Y. Suzuki, and A. A. Tulapurkar, Observation of thermally driven field-like spin torque in magnetic tunnel junctions, *Appl. Phys. Lett.* **109**, 032406 (2016).
- [17] A. Soumyanarayanan, N. Reyren, A. Fert, and C. Panagopoulos, Emergent phenomena induced by spin-orbit coupling at surfaces, and interfaces, *Nature (London)* **539**, 509 (2016).
- [18] C. F. Pai, L. Liu, Y. Li, H. W. Tseng, D. C. Ralph, and R. A. Buhrman, Spin transfer torque devices utilizing the giant spin Hall effect of tungsten, *Appl. Phys. Lett.* **101**, 122404 (2012).
- [19] A. R. Mellnik, J. S. Lee, A. Richardella, J. L. Grab, P. J. Mintun, M. H. Fischer, A. Vaezi, A. Manchon, E. A. Kim, N. Samarth, and D. C. Ralph, Spin-transfer torque generated by a topological insulator, *Nature (London)* **511**, 449 (2014).
- [20] W. Zhang, M. B. Jungfleisch, F. Freimuth, W. Jiang, J. Sklenar, J. E. Pearson, J. B. Ketterson, Y. Mokrousov, and A. Hoffmann, All-electrical manipulation of magnetization dynamics in a ferromagnet by antiferromagnets with anisotropic spin Hall effects, *Phys. Rev. B* **92**, 144405 (2015).
- [21] D. Macneill, G. M. Stiehl, M. H. D. Guimaraes, R. A. Buhrman, J. Park, and D. C. Ralph, Control of spin-orbit torques through crystal symmetry in WTe_2 /ferromagnet bilayers, *Nat. Phys.* **13**, 300 (2016).
- [22] K. Kondou, R. Yoshimi, A. Tsukazaki, Y. Fukuma, J. Matsuno, K. S. Takahashi, M. Kawasaki, Y. Tokura, and Y. Otani, Fermi-level-dependent charge-to-spin current conversion by Dirac surface states of topological insulators, *Nat. Phys.* **12**, 1027 (2016).
- [23] A. Bose, S. Dutta, S. Bhuktare, H. Singh, and A. A. Tulapurkar, Sensitive measurement of spin-orbit torque driven ferromagnetic resonance detected by planar Hall geometry, *Appl. Phys. Lett.* **111**, 162405 (2017).
- [24] A. Bose, H. Singh, S. Bhuktare, S. Dutta, and A. A. Tulapurkar, Sign Reversal of Fieldlike Spin-Orbit Torque in an Ultrathin Cr/Ni Bilayer, *Phys. Rev. Applied* **9**, 014022 (2018).
- [25] C. O. Avci, A. Quindeau, C. Pai, M. Mann, L. Caretta, A. S. Tang, M. C. Onbasli, C. A. Ross, and G. S. D. Beach, Current-induced switching in a magnetic insulator, *Nat. Mater.* **16**, 309 (2017).
- [26] B. F. Miao, S. Y. Huang, D. Qu, and C. L. Chien, Inverse Spin Hall Effect in a Ferromagnetic Metal, *Phys. Rev. Lett.* **111**, 066602 (2013).
- [27] H. Wang, C. Du, P. Chris Hammel, and F. Yang, Spin current and inverse spin Hall effect in ferromagnetic metals probed by $Y_3Fe_5O_{12}$ -based spin pumping, *Appl. Phys. Lett.* **104**, 202405 (2014).
- [28] T. Taniguchi, J. Grollier, and M. D. Stiles, Spin-Transfer Torques Generated by the Anomalous Hall Effect and Anisotropic Magnetoresistance, *Phys. Rev. Applied* **3**, 044001 (2015).
- [29] L. Liu, C. F. Pai, D. C. Ralph, and R. A. Buhrman, Current-Induced Switching of Perpendicularly Magnetized Magnetic Layers Using Spin Torque from the Spin Hall Effect, *Phys. Rev. Lett.* **109**, 186602 (2012).
- [30] S. Bhuktare, H. Singh, A. Bose, and A. A. Tulapurkar, Spintronic Oscillator Based on Spin-Current Feedback Using the Spin Hall Effect, *Phys. Rev. Applied* **7**, 014022 (2017).
- [31] H. Singh, K. Konishi, S. Bhuktare, A. Bose, S. Miwa, A. Fukushima, K. Yakushiji, S. Yuasa, H. Kubota, Y. Suzuki, and A. A. Tulapurkar, Integer, Fractional, and Sideband Injection Locking of a Spintronic Feedback Nano-Oscillator to a Microwave Signal, *Phys. Rev. Applied* **8**, 064011 (2017).
- [32] A. A. Tulapurkar, Y. Suzuki, A. Fukushima, H. Kubota, H. Maehara, K. Tsunekawa, D. D. Djayaprawira, N. Watanabe, and S. Yuasa, Spin-torque diode effect in magnetic tunnel junctions, *Nature (London)* **438**, 339 (2005).
- [33] H. Kubota, A. Fukushima, K. Yakushiji, T. Nagahama, S. Yuasa, K. Ando, H. Maehara, Y. Nagamine, K. Tsunekawa, D. D. Djayaprawira, N. Watanabe, and Y. Suzuki, Quantitative measurement of voltage dependence of spin-transfer torque in MgO -based magnetic tunnel junctions, *Nat. Phys.* **4**, 37 (2008).
- [34] T. Nozaki, Y. Shiota, S. Miwa, S. Murakami, F. Bonell, S. Ishibashi, H. Kubota, K. Yakushiji, T. Saruya, A. Fukushima, S. Yuasa, T. Shinjo, and Y. Suzuki, Electric-field-induced ferromagnetic resonance excitation in an ultrathin ferromagnetic metal layer, *Nat. Phys.* **8**, 491 (2012).
- [35] S. Miwa, S. Ishibashi, H. Tomita, T. Nozaki, E. Tamura, K. Ando, N. Mizuochi, T. Saruya, H. Kubota, K. Yakushiji, T. Taniguchi, H. Imamura, A. Fukushima, S. Yuasa, and

- Y. Suzuki, Highly sensitive nanoscale spin-torque diode, *Nat. Mater.* **13**, 50 (2014).
- [36] M. H. D. Guimaraes, G. M. Stiehl, D. MacNeill, N. D. Reynolds, and D. C. Ralph, Spin-orbit torques in NbSe₂/permalloy bilayers, *Nano Lett.* **18**, 1311 (2018).
- [37] S. Iihama, T. Taniguchi, K. Yakushiji, A. Fukushima, Y. Shiota, S. Tsunegi, R. Hiramatsu, S. Yuasa, Y. Suzuki, and H. Kubota, Spin-transfer torque induced by the spin anomalous Hall effect, *Nat. Electron.* **1**, 120 (2018).
- [38] S-h. C. Baek, V. P. Amin, Y. W. Oh, G. Go, S. J. Lee, G. H. Lee, K. J. Kim, M. D. Stiles, B. G. Park, and K. J. Lee, Spin currents and spin-orbit torques in ferromagnetic trilayers, *Nat. Mater.* **17**, 509 (2018).